Performance assessment of ferrite- and neodymiumassisted synchronous reluctance machines

Performance Assessment of Ferrite- and Neodymium-assisted Synchronous Reluctance Machines

Riccardo Leuzzi, Paolo Cagnetta, Francesco Cupertino
Politecnico di Bari
Department of Electric and Information Engineering
Bari, Italy
{riccardo.leuzzi, francesco.cupertino}@poliba.it

Simone Ferrari, Gianmario Pellegrino
Politecnico di Torino
DENERG – Department of Energy
Torino, Italy
{simone.ferrari, gianmario.pellegrino}@polito.it

***Abstract*—Growing attention towards environmental sustainability of energy conversion and stricter efficiency standards are encouraging the market penetration of high-efficiency electrical motors. Current regulations define international efficiency classes and the testing procedures for direct-on-line machines only, commonly induction motors. Synchronous reluctance machines are a valid alternative to the widely employed induction motors for variable-speed applications, due to their low manufacturing cost and higher efficiency. With proper design, torque ripple can be mitigated as much as to make rotor skewing unnecessary for most of applications. The low power factor downside can be fixed by inserting low-cost ferrite magnet into the rotor barriers, with benefits also on the torque capability and constant power speed range. The aim of this paper is to assess the performance and efficiency potential of one synchronous reluctance and two permanent magnet-assisted synchronous reluctance machine prototypes, obtained by replacing the rotor of a general-purpose induction motor with the said synchronous reluctance ones. The rotor barriers have been designed by means of a genetic optimization algorithm has and then adapted to insert commercially available magnets, compliant with minimum extra-cost requirements. The two prototypes were comprehensively characterized, to validate the design phase and to investigate the performance of the machines. The provided experimental results are critically examined and commented.**

Keywords—efficiency, electric motors, industrial applications, permanent magnets, IEC efficiency classes, NEMA premium efficiency, synchronous reluctance, testing procedures.

I. INTRODUCTION

Energy efficiency and long-term sustainability of the industry are compelling themes of global importance. Electric motor-driven systems account for almost 45% of the global consumption of electric energy. Mid- and large-sized motors with output power between 0.75 and 1000 kW represent the largest proportion of motor electricity in use today, accounting for 70% of the total industrial electricity demand [1]. This data shows the critical need of improving the average efficiency level of motors used in industrial applications to revert the actual trend, which would inevitably affect environment and resources availability in the near future. It is for this reason that governments in many countries have started the process of developing Minimum Efficiency Performance Standards (MEPS), towards the use of higher-efficiency motors in industrial systems. Within the European Union, MEPS are regulated by the IEC 60034-30-1 [2]. This standard defines four International Efficiency (IE) classes for single-speed motors designed for sinusoidal voltage operation comprised between 50 V and 1 kV, at constant line frequency, with 2,4,6 or 8 poles. The efficiency levels are defined as a function of the machine rated power, spanning a range between 120 W and 1000 kW; to assess the compliance to the standard, manufacturers have to perform efficiency tests according to the IEC 60034-2-1 [3]. The main limitation of current regulations relies in the fact that their application is limited to non-inverter-fed machines, so that no well-defined procedures exists for variable speed drives (VSD) and efficiency is not intended on a system level.

General-purpose induction motors (IMs) are today the most popular choice in industry, as a natural consequence of their robustness and low cost, backed by a well-established engineering expertise and the possibility of direct on-line (DOL) operation for fixed speed applications. With the diffusion of MEPS, manufacturers have enhanced IMs efficiency, ending up with IE3 and IE4 motors in their rosters. However, further improvements of the IM efficiency are impeded by technical limitations, such as the unavoidable rotor cage loss related to the asynchronous working principle. For variable-speed applications, DOL operation capability is unnecessary, and VSD made with synchronous motors lead to better efficiency and performance than the corresponding VSDs made with IMs. Among the synchronous machines family, synchronous reluctance (SyR) motors represent an appealing alternative because of several features:

- robustness and reliability
- low cost and ease of manufacturing
- higher efficiency than IMs due to the absence of rotor copper losses and easier cooling
- higher torque and power density than IM at same copper temperature
- possibility of flux-weakening [4]
- saliency-based encoderless control methods work robustly, due to the high saliency ratio [5].

An analytical comparison of the thermal behavior of a SyR machine and an IM can be found in [6], showing that the SyR motor is capable of 35% lower losses than the IM, in the sizes 2.2 - 4.0 kW. Conversely, if compared at same operating temperature, torque of the SyR is almost 20% higher, in the same frame size.

The main drawbacks of this technology are the lower power factor, respect to IMs, and the need of skewing to cancel the torque ripple, as it is commonly done for IMs. Many studies have addressed analytical and automated design criteria for SyR motors, demonstrating the key role of the flux barriers placement on the reduction of torque ripple and performance improvement [7-9]. The power factor problem could be fixed if the steel ribs that keep the rotor flux carriers together could be avoided or made non-magnetic, a matter that materials scientists are investigating [11]. With today's technology, inserting a limited quantity of permanent magnets (PM) into the rotor barriers saturates the rotor bridges thus cancelling their anti-reluctant action, and altogether improves the machine power factor and torque capability [12]. Such machines are commonly referred to as PM-assisted synchronous reluctance (PM-SyR).

In this paper, torque and efficiency performance of one SyR and two PM-SyR motors obtained by substituting the rotor of a commercial IM are indagated. The original motor was an IE3 low-voltage IM rated 1.1 kW at 1437 rpm, with a nameplate efficiency of 84.1% at full load. The adopted design procedure aims to a compromise between performance and cost: it first optimizes the rotor barriers to maximize efficiency at the same rated load of the IM, while also minimizing torque ripple. Secondly, the barriers' geometry is calibrated so to add commercial magnets of rectangular shape. Three prototypes have been designed and manufactured: one SyR, one Ferrite-SyR and one PM-SyR with NdFeB magnet. All three use identical rotor laminations. The stator laminations, winding arrangement, housing and cooling system have been kept the same of the IM. The intent of the study is twofold. On the one hand, it aims to assess the efficiency level that is achievable by simply substituting the rotor of an IE3 IM with a SyR type one. Secondly, the magnetic behaviour of low-cost ferrite magnets and high-energy NdFeB magnets is compared to show intrinsic performance differences.

II. Rotor Design Procedure

The adopted design procedure consists of three main steps:

1. barriers' number, position and shape are optimized for maximum torque per ampere and minimum ripple, according to the geometry of the original IM.
2. the magnets are designed so to meet the PM flux linkage requirement of the application, using a fictitious magnet of tunable remanence and occupying the entire flux barriers volume.
3. finally, the barriers are adapted to accommodate commercial magnet pieces, thus reducing manufacturing cost.

A. Barriers optimization

Before starting the design process, a necessary step was to retrieve geometrical and performance data from the original IM. Among these are rotor and stator dimensions, air-gap thickness, axial length, winding arrangement, rated current and friction and windage losses. Key parameters for the design of the new rotors are, above all, the shaft and rotor external diameters, and the stack length. Fig. 1 shows a picture of the stator cross section of the original IM. Main data are reported in Table I.

The rotor geometry was designed with the aid of multi-objective optimization algorithms to find the best compromise between average torque per joule loss and torque ripple. These performance indexes are mainly determined by the rotor lamination geometry: barrier shape and number of barriers per pole (called layers in the following), angular position on rotor periphery $\Delta\alpha_i$, and barrier thickness h_{ci}. Main optimization parameters are defined according to Fig. 2. The in-depth description of optimization algorithms is out of the scope of this paper; for those who were interested, more details can be found in [9]. In this paper, we limit our description to the conceptual steps that lead to the final geometry selection.

TABLE I. Parameters of the Designed Motors

Parameter	Value	Parameter	Value
Stator diameter (mm)	150.0	Number of turns per slot	54
Axial length (mm)	100.5	Number of parallel paths	2
Air-gap thickness (mm)	0.325	Number of barriers per pole	3
Rotor diameter (mm)	91.4	Barrier type	fluid
Stator slot number	36	Ferrite remanence (T)	0.41
Layers per slot	1	NdFeB remanence (T)	1.22

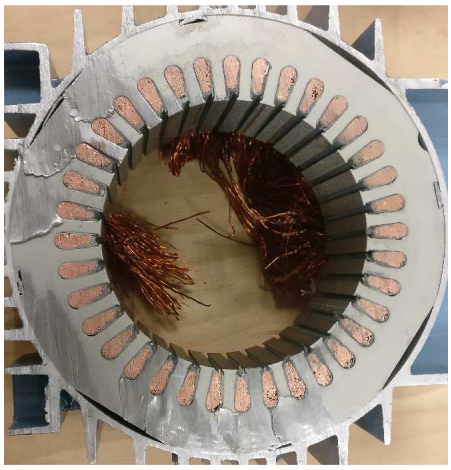

Fig. 1. Photo of a section-cut of the original IM stator

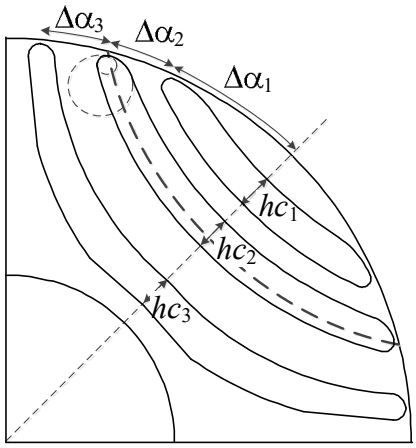

Fig. 2. Definition of barrier parameters

At a first step, several optimization runs were performed in order to investigate different possibilities for barrier shape and layer number. The number of layers investigated was limited to

three and five. Since the torque capability of the SyR machine is strictly related to the saliency ratio, which in turn is correlated to the number of barriers, it is intuitive that rotors with less than three layers would have lower torque performance. However, a high number of layers increases manufacturing complexity, with a limited increase in torque. Finite Element Analysis (FEA) plays a key role within the algorithm. To fully exploit its potential, the scripting capability of the open source software FEMM [16] has been used to automatically draw the barriers depending on the selected shape and layer number, according to a predefined range of variation for the geometric rotor parameters defined above. The result of the first optimization runs let us identify the best designs for each group.

Then, the best designs were verified for centrifugal forces at maximum speed and the feasible designs were studied in detail to find the one with the best compromise between efficiency and torque. At this stage, the selected machine was a rotor with three barriers per pole and geometry of the "fluid" type [15]. A second optimization run was then performed starting from the winning geometry and selecting finer parametric variations. The result was again verified for mechanical robustness, and it is the one reported in Fig. 3a.

B. Description of the optimal SyR rotor

The barrier profile that have been chosen is inspired to the field lines in a solid rotor, derived from the conformal mapping theory, as in [13,15]. To automatically build a fluid barrier starting at position $\Delta\alpha_i$, a mathematical expression of the associated field line must be used, which relates the polar coordinates of each point of the field line to the angular position of the barrier on the rotor periphery. Once the base profile has been calculated, the other optimization variables (i.e. h_{ci}) are used to determine barrier profile, according to properly selected constraints.

C. Magnet Design

The optimized SyR rotor is reported in Fig. 3a and referred to as the one with "original rotor layers". Last step in the design process is the sizing of magnet quantity to realize PM-SyR rotors. For the sake of simplicity, the barriers are initially supposed completely filled with a permanent magnet material having remanence B_r' and parallel magnetization direction, as indicated in Fig. 3b. The design parameter B_r' was calibrated to obtain a constant power speed range higher than 4:1. Different values of B_r' were simulated and the optimum in terms of constant power and torque level was found around a value of PM remanence of 0.13 T. A further increase of magnet strength would lead to a negligible power increase at low speed, associated to a significant power drop at maximum speed. Fig. 4 reports the output power characteristics of the three machines calculated from the experimentally identified magnetic model, confirming that the desired constant power speed range is achieved.

D. Barrier re-shaping for rectangular magnet

Unless cast bonded magnets are used, the solution of Fig. 3b is hardly manufacturable. A valid alternative is to replace the low-remanence bonded magnet with smaller pieces of higher strength magnetic material, namely rectangular pieces of commercial ferrite or NdFeB.

Say the volume of one barrier is V_r' and the remanence of the final magnet piece is B_r, the volume of the new magnet V_r can be found by the simple proportion $V_r = V_r' B_r' / B_r$. Following this principle, two PM-SyR rotors have been realized, one with ferrite BMHF-32/32 magnets ($B_r = 0.41\,T$) and one with BMN-38H NdFeB magnets ($B_r = 1.22\,T$). The original rotor layers were modified so to realize a rectangular slot, large enough to accommodate Ferrite magnets as shown in Fig 3b and referred as "modified rotor layers". Finally, radial ribs were added to avoid magnet displacement and to improve mechanical robustness. Their thickness was kept equal to the minimum tolerance allowed by the laser cut technology adopted to realize the prototypes. Three identical rotor stacks were manufactured according to the final design reported in Fig. 3b. One was left with no magnets, and the other two were used to realize one Ferrite PM-SyR rotor and one NdFeB PM-SyR rotor. Fig. 5 shows a picture of the three rotors. In principle, the three layers would need optimized quantities of magnet material. For cost and simplicity reasons, the magnet pieces of the two PM-SyR prototypes are the same for the three layers. Table II reports how the dimensions of the magnet pieces were calculated, after the initial design with all barriers filled at $B_r' = 0.13\,T$ remanence.

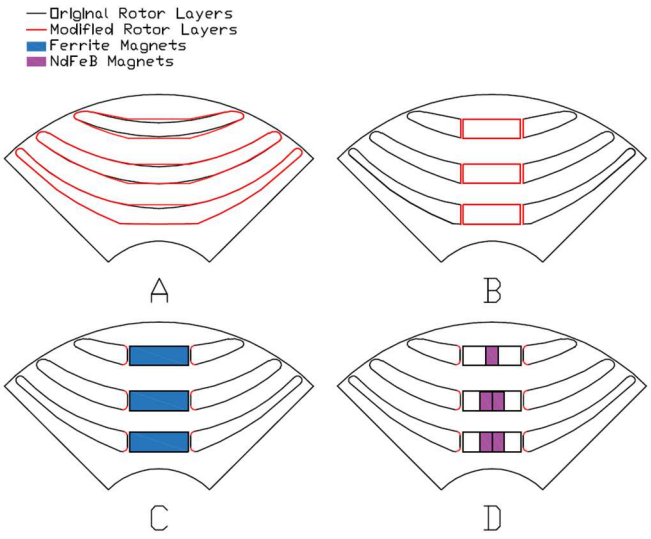

Fig. 3. Adaptation of barrier shape to insert the magnets: a) original, b) modified, c) with ferrite magnets, d) with NdFeB magnets.

TABLE II. SELECTION OF OPTIMAL MAGNET DIMENSIONS

Layer	**Layer area (mm^2)**	**Area of Hard Ferrite magnets (mm^2)**		**Area of NdFeB magnets (mm^2)**	
		Optimal	***Selected***	***Optimal***	***Selected***
1 (external)	95.24	30.95	48	10.15	10
2 (intermediate)	173.65	56.44	48	18.30	20 (2x10)
3 (internal)	182.13	59.19	48	19.41	20 (2x10)
		Weigthed Average Br = 0.1392 T (+7%)		Weigthed Average Br = 0.1354 T (+4%)	

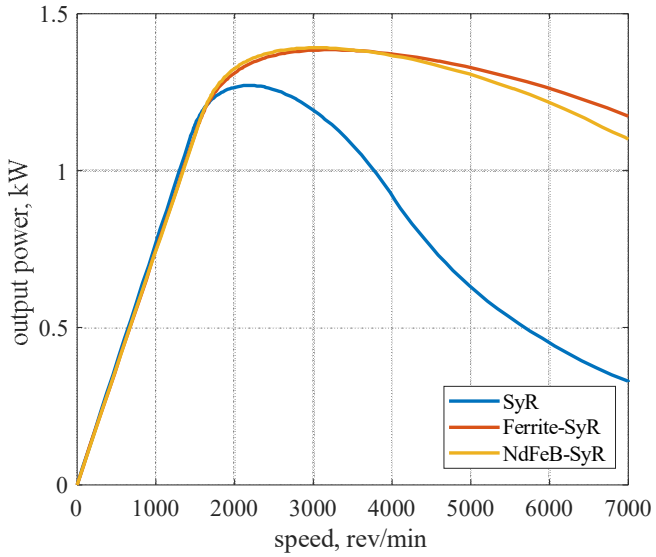

Fig. 4. Selection of magnet flux for the PM-assisted SyR motors.

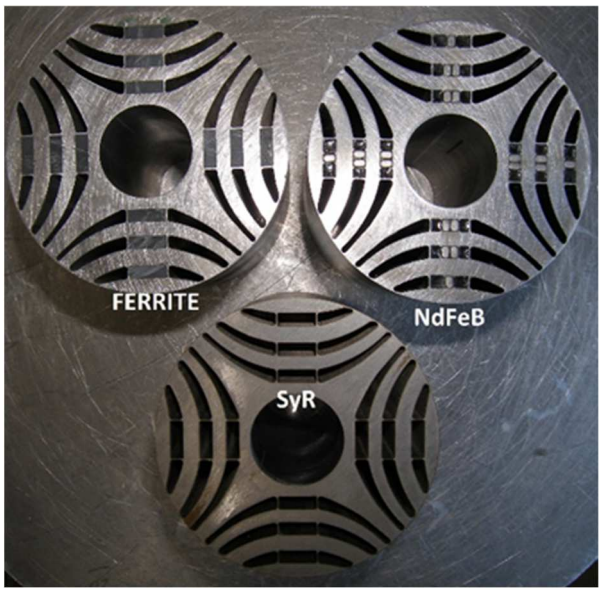

Fig. 5. Picture of the three rotors assembled.

Ferrite magnets have dimensions 12x4x10 mm^2, NdFeB magnets have dimensions 2.5x4x10 mm^2. To quantify the goodness of the approximation, a weighted remanence has been calculated, the error is 7% and 4% for the ferrite and NdFeB, respectively. The design parameters of the manufactured motor are reported in Table I.

III. Experimental Results

A. Description of the test procedures

A dedicated test rig was employed for the experimental validation procedure, composed of a speed controlled dynamometer machine (DM), a data recorder that measures phase currents, line-to-line voltages, shaft torque and speed of the machine under test (MUT) and an inverter to drive the MUT (Fig. 6). For both prototypes, these key tests were performed:

- Flux linkage map identification.
- Efficiency map.
- Thermal test under load.
- No load loss and mechanical loss measurement.

For each MUT, the flux tables were first identified. The flux curves allow finding the key control trajectories, such maximum torque per ampere and flux weakening control laws. The DM sets the speed at about one third of the rated speed of the machine (in order to make the iron loss effect negligible), while the MUT is current-controlled along a grid in the id-iq plane. Currents, voltages and position are measured for each point of the grid, and the flux linkages along the d- and q-axis are evaluated according to the procedure explained in [12], which consist of a symmetrical motor and brake sequence, used to compensate for the stator voltage resistance and evaluate the machine back-emf with adequate precision.

Second, the efficiency maps were measured. Each MUT is torque controlled, while the DM sets the speed. A grid of torque speed combinations is covered in the speed-torque plane. For each point, line-to-line voltages, phase currents, speed and torque of the MUT are measured, so to evaluate the efficiency. Winding resistance is estimated at regular time intervals during the test by zeroing the speed and measuring the voltages and currents of the MUT at half the rated torque (only resistance voltage). This is done to keep track of the thermal state of the motor comprehensively during the test, and allows precise compensation of stator copper loss, according to the actual temperature of the windings.

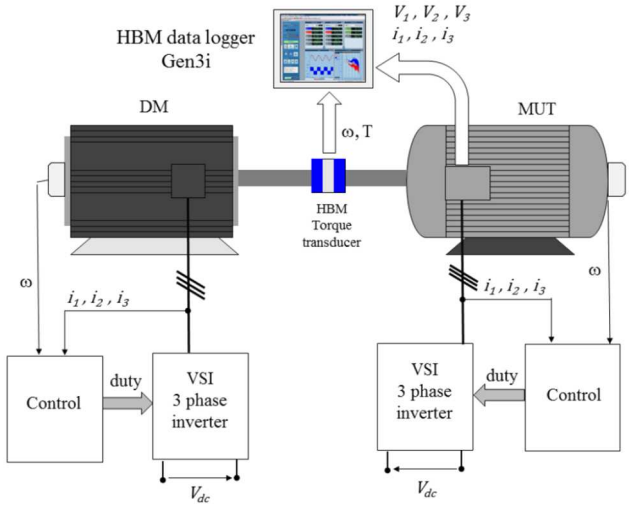

Fig. 6. Setup for characterization and testing of the prototypes.

B. Torque and magnetic analysis

First, the nominal current of the three prototypes is evaluated. The histogram in Fig. 7 compares the current needed by the machines to produce the rated torque of 7.1 Nm in MTPA conditions, or equivalently the torque capability for the same current of 2.7 Arms. Two observations can be made from the data shown in Fig. 7. The first one is that the SyR motor requires a higher current with respect to the IM to produce the same torque, about 7% more. This result is in line with the analysis presented in [6] by *Boglietti et alt.*, where a current increase of

about 10% was obtained for a 2.2 kW SyR motor with respect to an IM of same rating. It is worth noticing that, despite the lower torque per ampere ratio, SyR machines have no rotor copper losses, therefore a higher overall efficiency results, as it is shown in paragraph B of this section. The second point is that the rated current of the neodymium-assisted SyR is slightly higher than that of the ferrite-assisted one, despite magnet quantity in the two cases was chosen to reach the same performance. This difference can be more clearly visualized by looking at the magnetic model of the two machines. Fig. 8 shows a comparison between the d-axis fluxes of the three machines as a function of the d-axis current in a range between zero and two and a half times the rated current. The curves refer to the limit condition of zero q-axis current, thus no cross-coupling intervenes. As it can be seen, the ferrite-assisted SyR motor behaves similarly to the one without magnets, while the neodymium-assisted machine goes earlier into iron saturation, showing an overall lower flux level. To understand the cause of this phenomenon, the shaded plot of the flux density in the two rotors (Fig. 9) have been compared by FEA.

Let start looking at the magnetic condition at no load, Fig. 9a and 9b. Although similar equivalent remanence has been chosen during the design, the better distribution of the ferrite magnet in the barriers lead to a heavier saturation level in the radial iron ribs if compared with the neodymium ones. Therefore, it can be concluded that the q-axis inductance of the NdFeB-SyR is slightly higher than that of the Ferrite-SyR, which means that the q-axis flux will be higher for the same working point (i_d, i_q) while the d-axis flux will be lower.

This can be shown in Fig. 10, where the values of the d- and q-axis fluxes of the Ferrite-SyR and the NdFeB-SyR are compared. Fig. 9c and 9d show the magnetic condition in the rotor when the rated current is applied along the d-axis only. As it can be seen, also local saturation phenomena occur in the space between the barriers when neodymium magnets are used due to the higher energy they have. This effect also contributes to the lower flux this machine exhibit with respect to the ferrite one, making this last choice preferable from a magnetic point of view in addition to the cost factor.

Fig. 11 shows the expected torque waveforms of the three prototypes, evaluated with FEA, at rated current and two times the rated current, respectively, both in MTPA conditions. The three rotors are not skewed. This reduces the manufacturing cost of the machines and permits to evaluate the impact of torque ripple before skewing. Despite this choice, the peak-peak torque ripple for the SyR and NdFeB-SyR motors is about 5.5% of the average torque, at rated torque, confirming the goodness of the optimization algorithm.

A slightly worst behavior is noticeable in the ferrite-SyR, which has a torque ripple of 7.3%. This can be explained by looking at Table II, in fact the commercial amount of magnet chosen is the one that diverges the more from the optimal values. If needed by the application, skewing the rotor, as normally done for IMs, would mitigate torque pulsations to zero. When the current is doubled, torque oscillations also double, being slightly higher for the two OM-SyR motors. At the time of writing, experimental tests with an appropriate bench are being conducted to validate these results.

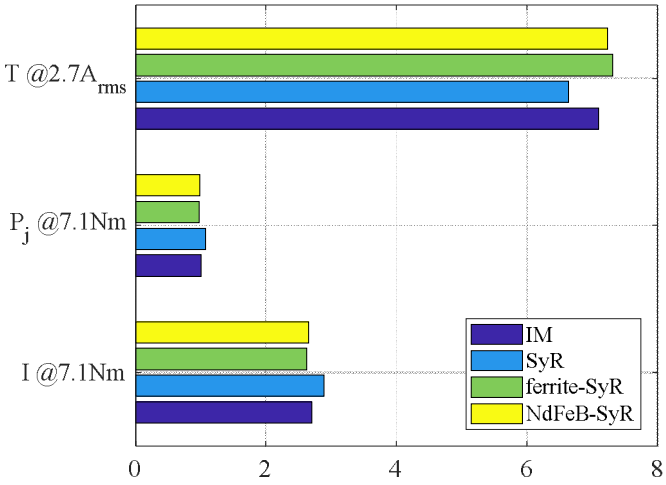

Fig. 7. Comparison of torque per ampere capability of the three prototypes and the original IM.

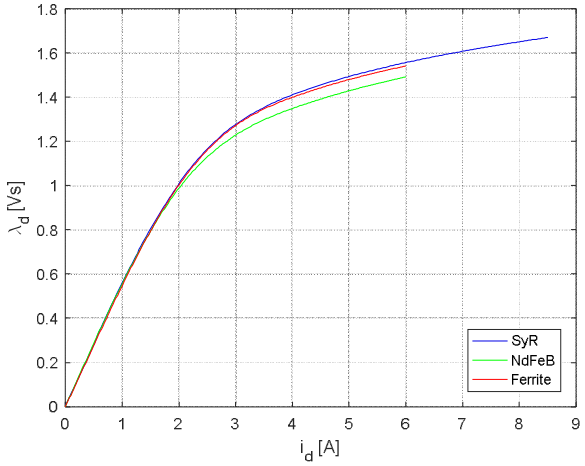

Fig. 8. Comparison of the d-axis flux linkage limit curves of the three prototypes.

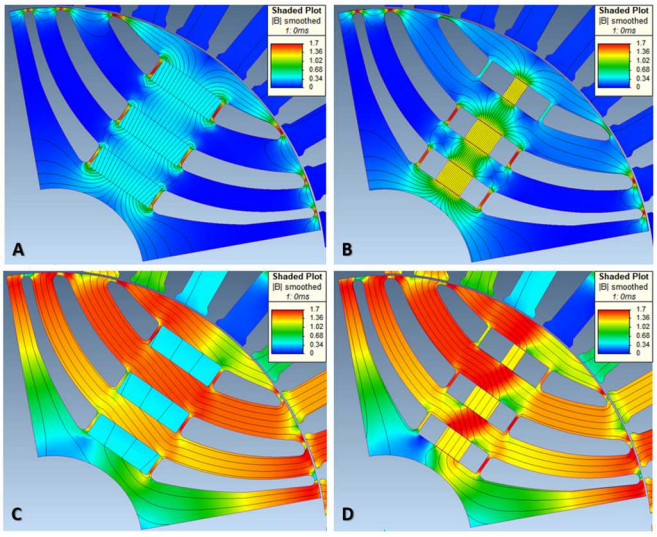

Fig. 9. Shaded plot of the magnetic flux density in the rotor of the two PM-SyR motors, at no load and rated d-axis current: a) ferrite, no load; b) neodymium, no load; c) ferrite, rated i_d; b) neodymium, rated i_d.

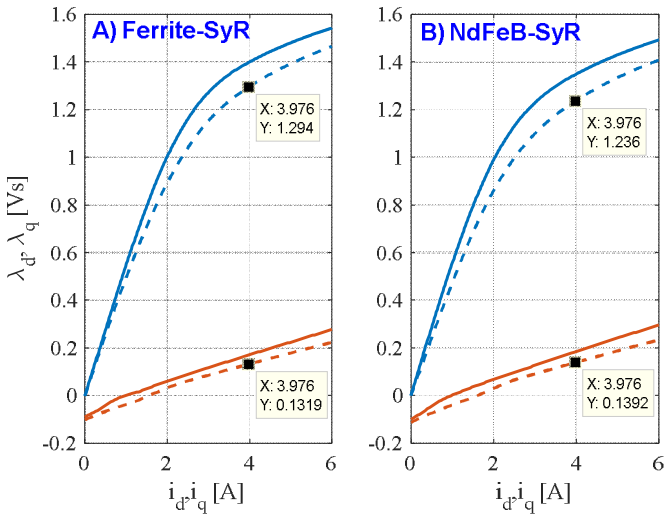

Fig. 10. Flux linkage curves of the two PM-SyR motors: $\lambda_d(i_d)$ is in blue, $\lambda_q(i_q)$ in orange; dashed curves refer to cross-coupling conditions, with 6 A on the other axis.

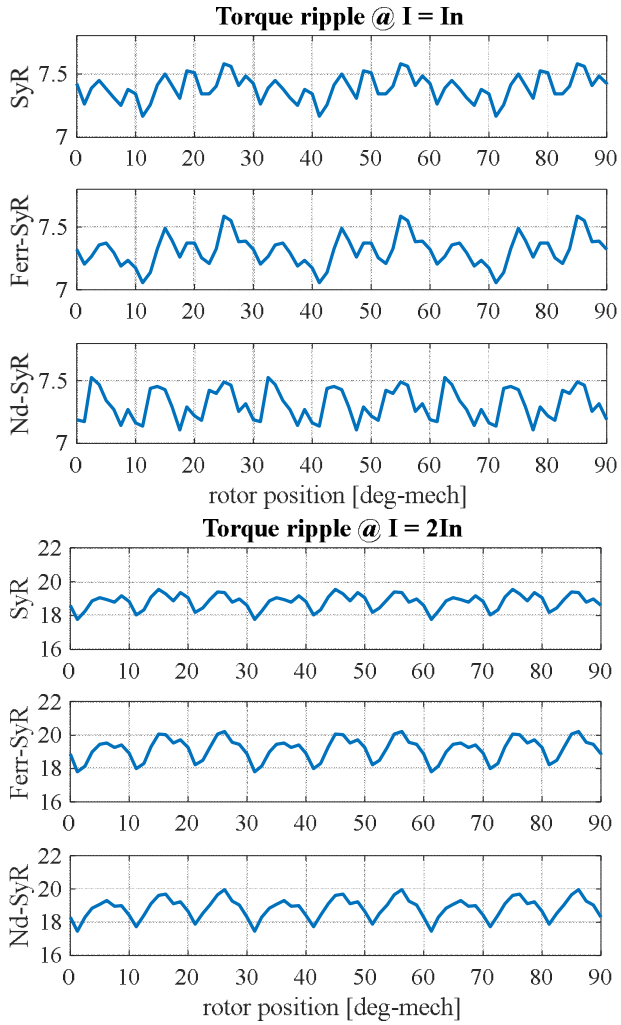

Fig. 11. FEA calculated torque waveforms of the three prototypes a) at rated torque; b) At 100% current overload.

C. *Efficiency*

Fig. 12 and 13 illustrate the efficiency maps of the SyR and of the NdFeB-SyR motors. The Ferrite-SyRM is not presented here since its map is very close to that of the NdFeB machine. The designed SyR motor has a rated efficiency of 85.0% (rated speed and load), while the two PM-SyR have 87.0%. Despite the SyR motor is just below the IE4 limit according to the standard IEC 60034-30-1 (minimum requirement is 87.2%), efficiency is a few points higher than the IM (84.1%). It has to be pointed out that the working principle of synchronous motors and the test procedure that have been employed here include the additional loss the machine produces because of the power converter. The IM, instead, is tested according to the IEC 60034-2-1 standard in DOL operation, as declared by the manufacturer. The measured efficiency of the IM falls at around 83.6% when this is driven by an inverter. Since the IEC standards admit a 15% tolerance on the measure of losses when evaluating efficiency, it can be assessed that the two PM-SyR can be classified as IE4 machines.

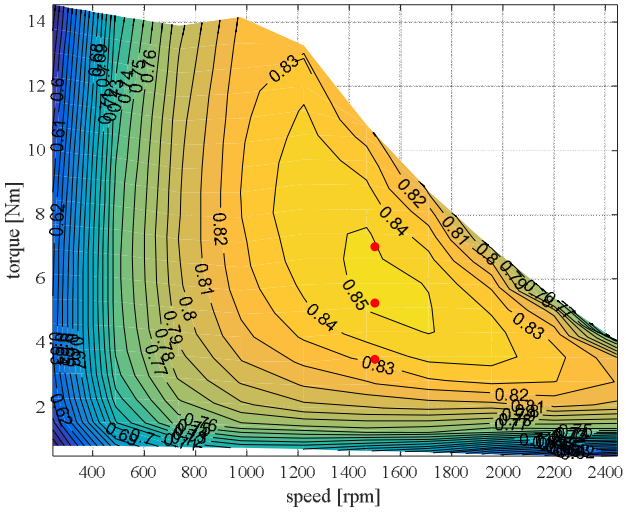

Fig. 12. Efficiency map of the SyR motor, In red, the points at 50%, 75% and 100% of rated torque.

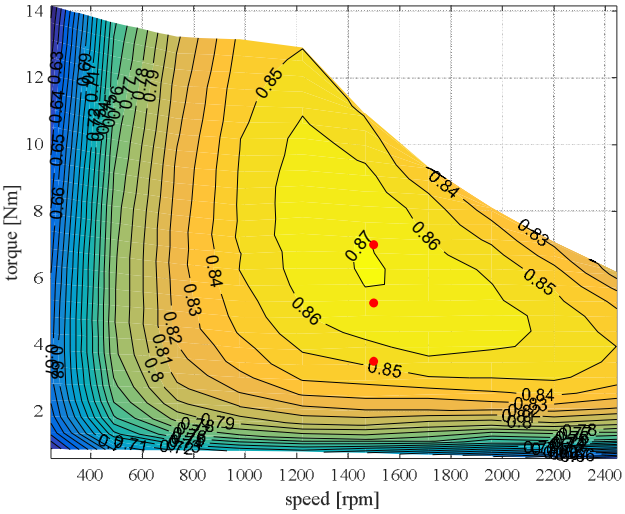

Fig. 13. Efficiency map of the NdFeB-assisted SyR motor, In red, the points at 50%, 75% and 100% of rated torque.

D. *Thermal test at nominal and maximum load*

The windings and permanent magnet temperatures were measured in steady-state conditions at rated speed, for 100% and 150% current levels. The results are reported in Fig. 14 and Fig.15 for the ferrite-assisted prototype. The magnet temperature was estimated by sampling the open circuit back-emf during the test, in dedicated timeframes where the current of the motor under test is set to zero for very limited time at regular instances. As expected in high efficiency motors, the temperatures are well below the maximum operating limits for copper and magnets at both rated and overload conditions. The higher temperatures are reached into the rotor at steady state. The overload capabilities of the ferrite assisted prototype benefits from the higher maximum operating temperature of ferrite magnets when compared to NdFeB ones.

IV. Conclusions and Future Work

This paper focused on performance analysis of three SyR and PM-SyR motors obtained by replacing the rotor of a commercial IE3 IM. The new SyR and PM-SyR rotors have been designed following an optimization procedure finalized at maximizing efficiency and reducing torque ripple. The design procedure also has the objective of reaching a trade-off between performance improvement in terms of efficiency and extended constant power speed range, cost minimization and manufacturing simplicity, considering the rotor barrier geometry and PM quantity. Results quantify the efficiency improvement that can be reached by a simple replacement of the rotor of a general-purpose high-efficiency IM with a SyR or PMa-SyR rotor. Practical issues related to the reduction of manufacturing cost and improvement of the structural integrity of the synchronous rotors have been addressed It has been also demonstrated that the machine with ferrite magnet not only reduces the cost but also improves the performances (particularly at overload) in terms of torque per ampere capability thanks to a reduction of local saturation phenomena that occur using high strength magnets.

Ongoing research activity is focusing on the impact of the control strategy (vector or scalar control and the selection of the flux level) on the performances of the considered synchronous and induction machines.

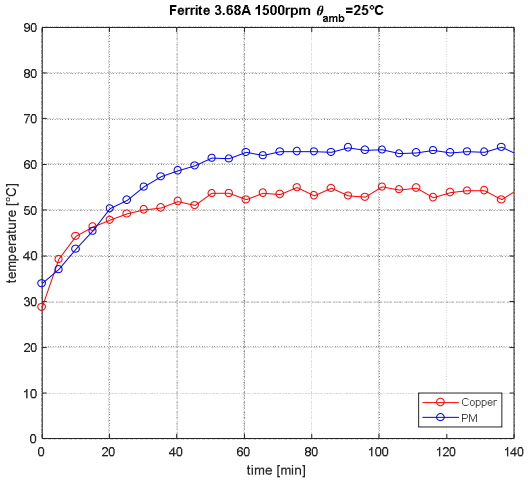

Fig. 14. Thermal settling of the coil and PM temperature in the ferrite-assisted SyR motor, at rated speed and rated current.

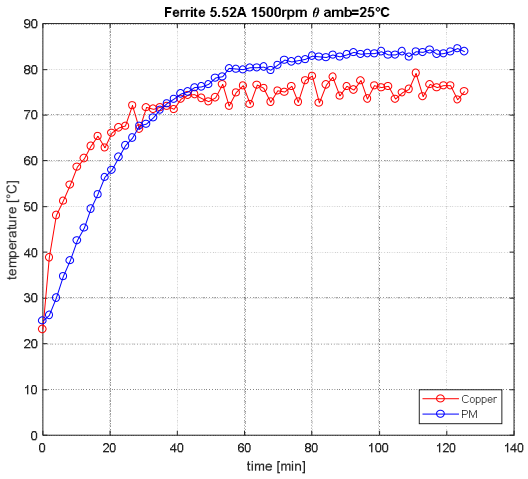

Fig. 15. Thermal settling of the coil and PM temperature in the ferrite-assisted SyR motor, at rated speed and 1.5 times the rated current.

References

[1] P Waide and C. U. Brunner, "Energy-Efficiency Policy Opportunities for Electric Motor-Driven Systems," *OECD Publ.*, 2011.

[2] Rotating electrical machines - Part 30-1: Efficiency classes of line operated AC motors (IE code), *IEC Standard 60034-30-1*, 2014.

[3] Rotating electrical machines - Part 2-1: Standard methods for determining losses and efficiency from tests (excluding machines for traction vehicles), *IEC Standard 60034-2-1*, 2014

[4] W. L. Soong and T. J. E. Miller, "Field-weakening performance of brushless synchronous AC motor drives," in *IEE Proceedings - Electric Power Applications*, vol. 141, no. 6, pp. 331-340, Nov 1994.

[5] M. Harke, H. Kim and R. D. Lorenz, "Sensorless control of interior permanent magnet machine drives for zero-phase-lag position estimation," *IEEE Transaction on Industry Applications*, vol. 39, no. 12, pp. 1661-1667, Nov./Dec. 2003.

[6] A. Boglietti, A. Cavagnino, M. Pastorelli and A. Vagati, "Experimental comparison of induction and synchronous reluctance motors performance," *Fourtieth IAS Annual Meeting. Conference Record of the 2005 Industry Applications Conference*, 2005, pp. 474-479 Vol. 1.

[7] A. Vagati, G. Franceschini, I. Marongiu and G. P. Troglia, "Design criteria of high performance synchronous reluctance motors," Conference *Record of the 1992 IEEE Industry Applications Society Annual Meeting*, Houston, TX, 1992, pp. 66-73 vol.1.

[8] A. Vagati, M. Pastorelli, G. Francheschini and S. C. Petrache, "Design of low-torque-ripple synchronous reluctance motors," in *IEEE Transactions on Industry Applications*, vol. 34, no. 4, pp. 758-765, Jul/Aug 1998.

[9] G. Pellegrino, F. Cupertino and C. Gerada, "Automatic Design of Synchronous Reluctance Motors Focusing on Barrier Shape Optimization," in *IEEE Transactions on Industry Applications*, vol. 51, no. 2, pp. 1465-1474, March-April 2015.

[10] M. Di Nardo et al., "End barrier shape optimizations and sensitivity analysis of synchrnous reluctance machines," *IECON 2015 - 41st Annual Conference of the IEEE Industrial Electronics Society*, Yokohama, 2015, pp. 002914-002919.

[11] P. B. Reddy, A. El-Refaie, S. Galioto and J. P. Alexander, "Design of synchronous reluctance motor utilizing dual-phase material for traction applications," *2015 IEEE Energy Conversion Congress and Exposition (ECCE)*, Montreal, QC, 2015, pp. 4812-4819.

[12] N. Bianchi, E. Fornasiero and W. Soong, "Selection of PM Flux Linkage for Maximum Low-Speed Torque Rating in a PM-Assisted Synchronous Reluctance Machine," in *IEEE Transactions on Industry Applications*, vol. 51, no. 5, pp. 3600-3608, Sept.-Oct. 2015.

[13] R. R. Moghaddam, "Synchronous reluctance machine (SynRM) in variable speed drives (VSD) applications," Ph.D. dissertation, KTH School of Elect. Eng., RIT, Stockholm, SW, 2011.

[14] E. Armando, R. I. Bojoi, P. Guglielmi, G. Pellegrino and M. Pastorelli, "Experimental Identification of the Magnetic Model of Synchronous Machines," in *IEEE Transactions on Industry Applications*, vol. 49, no. 5, pp. 2116-2125, Sept.-Oct. 2013.

[15] M. Gamba, G. Pellegrino and F. Cupertino, "Optimal number of rotor parameters for the automatic design of Synchronous Reluctance machines," *2014 International Conference on Electrical Machines (ICEM)*, Berlin, 2014, pp. 1334-1340.

[16] David Meeker, Finite Element Method Magnetics [Online]. Available: http://www.femm.info.